

THE UNIVERSITY OF CHICAGO

MASTER'S THESIS

**DISKWORLD: Modeling the Role of Tectonic
Collisions in Long-Term Climate Stability**

Author:
Brandon Park COY

Supervisor:
Dr. Edwin S. KITE



*A thesis submitted in fulfillment of the requirements
for the degree of Master of Science*

in the

Physical Sciences Division

May 24, 2022

Abstract

DISKWORLD: Modeling the Role of Tectonic Collisions in Long-Term Climate Stability

The carbonate-silicate weathering feedback cycle is thought to stabilize Earth's atmospheric CO₂ inventory and climate on geologic ($> 10^6$ yr) timescales. If the climate warms, increased mineral dissolution rates and increased global precipitation cause silicate weathering rates to increase, thereby increasing CO₂ drawdown and counteracting the initial warming. Limits to where this feedback cycle can conceivably operate on the surface of terrestrial planets with N₂–O₂–CO₂–H₂O dominated atmospheres have been used to define the 'liquid water habitable zone'—where water can exist on a planet's surface for geologic timescales. The feedback cycle is reliant on tectonic activity and other processes in order to resupply silicate minerals available for weathering. Without resupply, rocks become leached of cations required for the drawdown of CO₂ and the feedback's strength decreases over time. Lower feedback strength increases a planet's susceptibility to inescapable runaway greenhouse or 'snowball' events where the planet's surface becomes completely frozen over. Little work has been done to quantify exactly what affects a planet's climate stability in spite of the randomness of tectonic activity. In this work, we present an idealized model meant to quantify long-term climate stability of abiotic Earth-like atmospheres—titled DISKWORLD. The model tracks the evolution of CO₂ concentration in the atmosphere as randomized 'plates' collide with each other and supply new weathering minerals. Through tracking the evolution of ocean pH and global temperatures, we can quantify the planet's susceptibility to runaway greenhouse and snowball events. By running our model with a variety of tectonic setups over 500 Ma timescales, we find that, in addition to frequent tectonic collisions spurred by a large fraction of the planet's surface being covered by continental plates, additional processes that either affect global CO₂ drawdown (e.g. seafloor weathering) or resupply fresh minerals for carbonate-silicate weathering (e.g. dust and glacial soil transport) are conducive in stabilizing climate on geologic timescales.

Acknowledgements

Thank you to the University of Chicago's Master of Science in the Physical Sciences Division program for giving me the opportunity to survey some of the cutting-edge research being performed in planetary sciences. Thank you to all of the wonderful professors in the Geophysical Sciences Division that made my time in the classroom challenging and exciting. Special thanks to my advisor Dr. Edwin Kite who helped ignite my interests in planetary habitability, and his group's members Sasha Warren, Bowen Fan, Xuan Ji, and Charlie Willard for helping in my transition to the field.

Contents

Abstract	ii
Acknowledgements	iii
1 Introduction	1
2 The Carbonate-Silicate Weathering Feedback	3
2.1 The WHaK Model	4
2.2 The MaC Model	4
3 Methods and Model Description	6
3.1 Disks	6
3.2 Precipitation and Runoff	6
3.2.1 Latitudinal Dependence	7
3.3 SiO ₂ fluxes and CO ₂ Consumption	8
3.4 Time Evolution	9
3.5 Climate Catastrophes	10
3.5.1 Runaway Greenhouse	10
3.5.2 Snowball events	10
3.6 Non-Tectonic Weathering Processes	11
3.6.1 Seafloor Weathering	11
3.6.2 Dust Transport	11
3.6.3 Physical Erosion and Glaciers	11
3.6.4 A Maximum Effective Soil Age $T_{s,max}$	12
4 Results	13
4.1 Trial Parameters	13
4.2 No $T_{s,max}$ Case	13
4.3 $T_{s,max}$ Case	13
4.4 Model Biases	18
5 Conclusion	20
5.1 Model Limitations and Future Work	20
5.1.1 Ice Albedo Feedback and $T(pCO_2)$	20
5.1.2 Precipitation and Runoff	20
5.2 Paleoreconstructions	21
A Appendix	22
A.1 pCO ₂ and Global Temperatures	22
A.2 CO ₂ Partitioning and Ocean Chemistry	24
A.3 MaC Model Temperature and pCO ₂ Dependencies	26
Bibliography	27

Chapter 1

Introduction

The carbonate-silicate weathering feedback, first proposed by Walker, Hays, and Kasting [40] (WHaK) as Earth’s climate regulator, has long been argued as the primary reason that Earth’s surface temperature has remained ‘habitable’—hospitable to the presence of surface liquid water—over the majority of its history (possibly as early as ~ 4.4 Gya [41]). Numerous studies have used the bounds of where this feedback cycle can conceivably operate on terrestrial planets with N_2 – O_2 – H_2O – CO_2 dominated atmospheres to define the limits of the ‘habitable zone’ of extrasolar planets [22].

Without a fast-acting (on timescales ~ 100 ky) negative feedback on changes in Earth’s temperature, the habitability of its surface would quickly become jeopardized by perturbations in incoming solar radiation (ISR) or volcanic outgassing of CO_2 [40, 39]. Thus, understanding the limits of this feedback cycle is crucial in determining which exoplanets are truly ‘habitable’ to complex life as we know it on geologic timescales.

The feedback counteracts the release of carbon dioxide gas (CO_2) into the atmosphere through CO_2 drawdown spurred by the interaction of exposed silicate rocks with water (referred to as ‘weathering’). Greenhouse gases like CO_2 increase Earth’s surface temperature by reemitting some of the outgoing longwave radiation (OLR) emitted by the planet back and using it to reheat the surface. The presence of greenhouse gases is required to sustain liquid water at Earth’s surface temperature, as Earth’s predicted surface temperature without the presence of an atmosphere is -18°C . The atmospheric greenhouse gas reservoir is volatile and can be perturbed by changes and imbalances in globally integrated weathering or volcanic outgassing fluxes. In extreme cases, high greenhouse gas concentrations can lead to a runaway greenhouse effect where a planet’s surface oceans are completely evaporated and temperatures rise to levels uninhabitable to any known forms of life. Low concentrations of CO_2 can lead to ‘snowball’ events where the entire surface layer of a planet’s oceans and land are frozen over. Little work has been done to quantify exactly what planetary parameters are important in determining a planet’s stability despite the randomness of weathering perturbations. Key open questions include: How does land fraction of a planet affect its resilience to perturbations in weathering flux? How does the magnitude of volcanic outgassing of CO_2 from a planet’s interior affect its long term climate stability? Are planets with no processes that affect weathering other than tectonic uplift from collisions stable on geologic timescale?

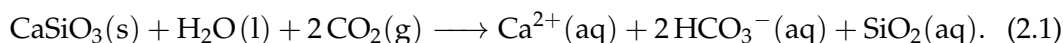
In this work we present a idealized model to test the strength of the carbonate-silicate weathering feedback presented in Maher and Chamberlain [28] against the randomness of continental plate collisions over geologic timescales, titled DISKWORLD. In Chapter 2 we present a high-level overview of the carbonate-silicate weathering feedback and discuss mathematical formulations outlined in two different well-vetted weathering models. In Chapter 3 we present concepts and formulae used in

the DISKWORLD model. In Chapter 4 we discuss the results of our simulations over a wide variety of possible tectonic setups. In Chapter 5 we present our conclusions and discuss possible future work regarding the role of tectonic collisions in climate stability.

Chapter 2

The Carbonate-Silicate Weathering Feedback

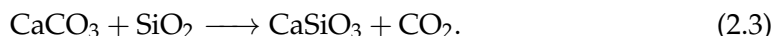
While many different types of silicate minerals participate in weathering, wollastonite (CaSiO_3) is often used to represent the underlying chemical reactions for stoichiometric simplicity. In reality, CaSiO_3 is not a significant contributor to silicate weathering on Earth's surface. Exposed silicates are dissolved via rainwater through reactions such as the following,



The aqueous products are then transported to the ocean via river runoff. If the ocean is saturated with respect to calcium carbonate (CaCO_3), which is the case for Earth's ocean [46], bicarbonate ion and calcium ion can recombine via carbonate precipitation,



Thus the net result of Reactions 2.1 and 2.2 is the removal of one molecule of CO_2 from the atmosphere in the form of CaCO_3 . A portion of the CaCO_3 eventually settles onto the seafloor and is subducted into Earth's mantle, where it is combined metamorphically with SiO_2 is released back as CO_2 into the atmosphere via volcanism:



The balances between the fluxes associated with Reactions 2.1/2.2 and 2.3 ultimately control the amount of inorganic carbon in the ocean plus atmosphere 'slow carbon' system. Imbalances in these fluxes have been tied to some of Earth's most catastrophic extinction events as well as the onset of 'Snowball Earth' episodes—periods of time where Earth's surface may have been mostly frozen over [23, 19, 6]. The most well-studied of these events in the Paleocene-Eocene Thermal Maximum (~ 55 Mya), which has been associated with a massive release of inorganic carbon into the atmosphere over a short (20 \sim 50 ky) timescale and led to the extinction of up to 50% of seafloor foraminifera [38, 44, 4]. It is still highly debated whether the majority of these climate-destabilizing events were caused by changes in volcanic outgassing (source-driven) or weathering fluxes (sink-driven) [10]. In this work, we explore susceptibility to sink-driven events.

Reaction 2.1 is sensitive to various surface processes on Earth, including localized rainfall/evaporation and the amount of fresh silicate rocks provided by tectonic uplift. Without tectonic activity or other processes resupplying fresh minerals, soil

would become leached of reactants for the drawdown of CO₂ in Reaction 2.1, and atmospheric CO₂ levels would quickly become large enough to trigger a runaway greenhouse effect that would evaporate Earth's oceans and make the surface of Earth uninhabitably hot, similar to what may have happened on Venus [21]. When a large amount of weathering minerals is introduced into the system through continental collisions, the opposite may occur, where low CO₂ concentrations would cause the majority of Earth's oceans freeze over.

2.1 The WHaK Model

Walker, Hays, and Kasting [40] presented a set of equations meant to explain global weathering estimates from river catchments and provide a negative feedback capable of keeping Earth's climate stable on geologic timescales. In this model, the amount of silicate rock weathering, W (t/km²/yr), is limited by the amount of river runoff, q , as well as a moderate temperature T and partial pressure of CO₂ (pCO₂) dependence:

$$W = kqe^{\frac{T-T_0}{13.4}} \left(\frac{p\text{CO}_2}{p\text{CO}_{2,0}} \right)^{0.3}, \quad (2.4)$$

where k is a weatherability factor that varies for different climates and lithologies and is reliant on fits to empirical data. Variations of this simple relationship have been used in a variety of Earth-history and exoplanet habitability-based studies, including paleoreconstructions of Earth's past CO₂ inventory (e.g. [10, 11]) and testing the model's sensitivity to various parameters like land fraction [13]. Equation 2.4 inherently contains a negative stabilizing feedback—if pCO₂, temperature, or precipitation increases, the amount of weathering will increase, increasing CO₂ drawdown, thereby lowering pCO₂ and subsequently temperature and precipitation.

2.2 The MaC Model

Maher and Chamberlain [28] (MaC) present a 'solute transport model' to help explain the underlying kinetics and kinematics governing the carbonate-silicate weathering feedback. Their analysis is also based on observed weathering flux and runoff values for various river catchments around the world.

In their model, the weathering flux of minerals to the ocean is related to the ratio of the mean fluid travel time through a reactive assemblage ($T_f \approx L\phi/q$) to the time required to reach equilibrium ($T_{eq} \approx C_{eq}/R_n$), where solute concentration in the river reaches a thermodynamic 'maximum concentration' C_{eq} . L is the reactive path length that rainwater travels through, ϕ is the porosity of the soil, and R_n is the reaction rate.

$R_n = \rho_{sf}k_{eff}AX_r f_w$, where ρ_{sf} is the ratio of solid mineral mass to fluid volume, A is the specific area for the minerals in question, X_r is the fraction of reactive material in fresh (unweathered) rock, k_{eff} is the weathering rate constant, and f_w is the fraction of fresh rock in the assemblage. $f_w = (1 + mk_{eff}AT_s)^{-1}$ where T_s is the effective soil age (or soil residence time) and m is the molar mass of the weathering minerals. The ratio of these two timescales, T_f/T_{eq} , is known as the 'Damköhler number' [3].

Maher and Chamberlain [28] introduce a similar quantity known as the ‘Damköhler coefficient’, which relates to the efficiency of solute production and is defined as

$$D_w = \frac{L\phi}{T_{eq}} = \frac{L\phi\rho_{sf}k_{eff}AX_r}{C_{eq}(1 + mk_{eff}T_s)}. \quad (2.5)$$

D_w is conceptually similar to the constant k presented in the WHaK model, as it varies over different climates and lithologies, from cratons ($D_w \sim 0.01$ m/yr) to mountain ranges ($D_w \sim 0.3$ m/yr). Maher and Chamberlain [28] use this coefficient to calculate the weathering flux of aqueous silica (SiO_2), W (t/km²/yr), where

$$W = Cq = C_{eq} \frac{e^2 D_w}{1 + e^2 D_w / q}. \quad (2.6)$$

where e is Euler’s constant.

In the high D_w limit (solutes are quick to reach equilibrium concentrations), $W \approx C_{eq}q$ and weathering becomes *transport limited* by precipitation as predicted by Equation 2.4. Conversely, in the low D_w limit $W \approx C_{eq}e^2 D_w$, and weathering becomes *kinetically limited* by D_w , asymptotically approaching $C_{eq}e^2 D_w$ as $q \rightarrow \infty$.

One important feature of Equation 2.6 is that it does **not** have an explicit reliance on the temperature of the system. Although temperature does have a direct effect on the kinematics of the dissolution reactions and the determination of k_{eff} , Maher and Chamberlain [28] claim that these effects are negligible and that weathering is primarily a function of soil properties and local runoff (the validity of these assumptions is explored in Appendix A.3). Thus the negative stabilizing feedback relies on the assumption that global precipitation will increase with increasing temperatures (discussed in Section 3.2), and higher values of D_w increase the system’s feedback strength.

One of the main advantages of the MaC model is that we are able to study the time-evolution of weathering fluxes in aging soils. Previous implementations of the WHaK model assume that weathering is primarily constrained by local climate types and not soil properties. Godderis et al. [11] use somewhat arbitrary bounds of local temperature and runoff to define ‘warm’, ‘mild’, ‘cold’, ‘humid’, ‘arid’, and ‘temperate’ climate states that uniquely determine k used in Equation 2.4 and vary by up to a factor of 14. Such empirical fits to k also do not conserve mass, as k should decrease over time as the local rock is leached of silicate minerals assuming there is no background resupply mechanism. Varying soil ages allow us to simulate the effects of tectonic activity and other processes that restore minerals for the carbonate-silicate weathering cycle. For these reasons, our model uses equations presented in the MaC model to test our hypotheses.

Chapter 3

Methods and Model Description

The model is meant to test how a system with an initially steady-state balance of volcanic outgassing and weathering sequestration of CO_2 responds to long-term evolution and short-term perturbations in weathering fluxes. Various parameters in the model are adjustable, and the model is applicable to planets with Earth-like continental plate sizes/numbers and those with different plate configurations.

3.1 Disks

We assume that the planet of interest is Earth-sized, represented by a sphere with radius $R_p = R_\oplus$. Disks are defined as circular plates with radius R , randomized velocities with mean speed V and standard deviation $\sigma = V/2$, and randomized starting locations. Collisions between disks do not alter their topographies and velocities remain constant over time.

To keep track of various properties, disks are sub-divided into an adjustable number of equiareally spaced points. The positions of these points are kept track of and they comove with the disk's center. Points are considered 'colliding' when they are contained within the boundaries of another disk. Collisions reset the effective age of the point to a specific number, $T_{s,reset}$, simulating the uplift of new soil and creation of mountain belts caused by plate collisions. Points that are not colliding age with the simulation. We run two scenarios—one in which points can age indefinitely and one in which they age until they reach an effective maximum age (see Section 3.6.4).

$T_{s,reset}$ was determined by fitting T_s in Equation 2.5 to the D_w value cited in Maher and Chamberlain [28] for mountain-like terrain, 0.3, using default parameters. This leads to a value of $T_{s,reset} \approx 3000$ yr.

3.2 Precipitation and Runoff

The MaC model carbonate-silicate weathering feedback has a large reliance on the assumption that globally-averaged rainfall generally increases as Earth's surface temperature increases. This happens due to increasing evaporation rates that balance precipitation in a state-steady. Following Graham and Pierrehumbert [13], we use a simplified linear relationship to define our globally averaged precipitation's (\bar{p}) temperature dependence:

$$\bar{p} = \bar{p}_{ref}(1 + \epsilon(T - T_{ref})), \quad (3.1)$$

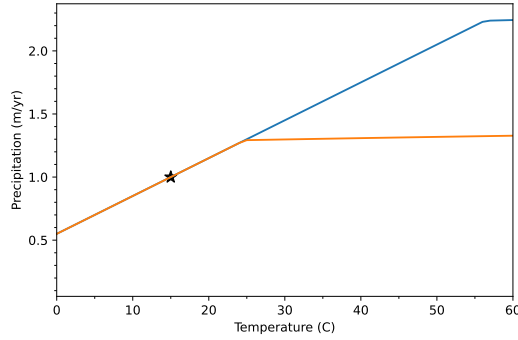


FIGURE 3.1: Globally averaged precipitation curves for Earth-like planets with land fraction $\gamma = 0.3$ (blue) and $\gamma = 0.6$ (orange) based on Equations 3.1 and 3.3. Planets with higher land coverage reach precipitation saturation at much lower temperatures and are thus more inherently susceptible to climate instabilities.

where T is the globally averaged surface air temperature and ϵ is the fractional change in precipitation per change in temperature measured at a reference temperature and precipitation value. \bar{p}_{ref} and T_{ref} represent modern-day Earth conditions, where $\bar{p}_{ref} \approx 1$ m/yr [45] and $T_{ref} = 15^\circ\text{C}$. We assume $\epsilon = 0.03$ following Graham and Pierrehumbert [13]. We also take runoff q to be a linear function of precipitation:

$$q = \Gamma p, \quad (3.2)$$

where Γ is a measured proportionality constant, often referred to as the ‘runoff coefficient’. $(1 - \Gamma)$ represents the amount of precipitation lost to evaporation before being converted to runoff. We use a globally averaged value of $\Gamma = 0.259$ based on globally integrated runoff estimates calculated in Ghiggi et al. [9].

We also include a maximum global precipitation based on Graham and Pierrehumbert [13], including their dependence on the land fraction of the planet γ ,

$$\bar{p}_{lim} = \frac{(1 - \gamma)(1 - \alpha)ISR}{L(T)4} \quad (3.3)$$

$$L(T) = 1.918 \times 10^9 \left(\frac{T}{T - 33.91} \right)^2 \quad (3.4)$$

where L is the latent heat of vaporization of water (in J/m^3) given by the Henderson-Sellers equation [17] and α is the planetary albedo, which we keep constant as $\alpha = 0.3$. Example precipitation curves can be seen in Figure 3.1.

3.2.1 Latitudinal Dependence

Previous measurements of present-day precipitation (e.g. Xie and Arkin [45]) and simulations using idealized generalized circulation models (GCMs, e.g. O’Gorman and Schneider [29] and references therein) have shown that latitude also has a significant impact on the local yearly averaged rainfall. While Earth’s latitudinal distribution is a complex function of land coverage, ocean heat transport, and atmospheric circulation, we use a simplified latitudinal dependence on rainfall/runoff,

$$q(\Phi) = 2\bar{q} \cos \Phi, \quad (3.5)$$

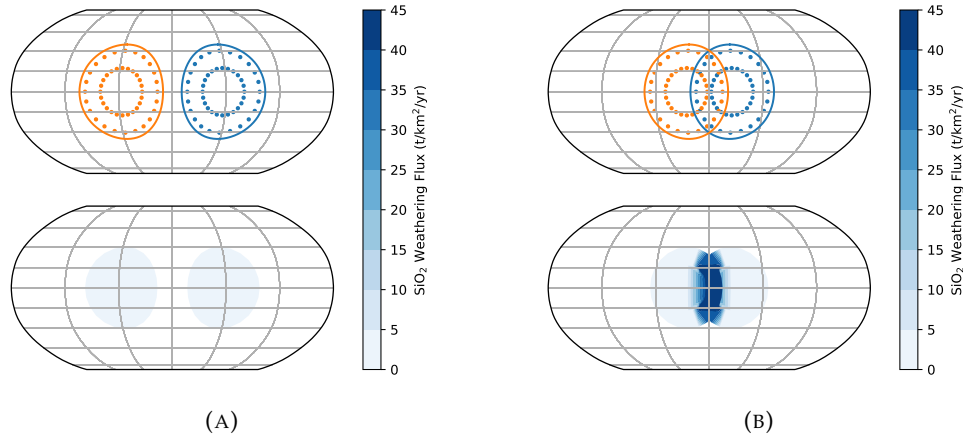


FIGURE 3.2: An example head-on collision at $\Phi = 0$ of two plates with $R = 5600$ km and associated changes in weatherability. Solid lines represent the actual boundaries of the plates, whereas points represent the equiareal grid points described in Section 3.1. Non-colliding terrain is set at a constant soil age of $T_s = T_{s,max}$. $T_{s,max}$ is described in Section 3.6.4. The creation of mountain ranges via tectonic uplift in (B) increases local weathering flux by a factor of 20, increasing global CO_2 drawdown.

where Φ is the latitude. This ensures a global average runoff of \bar{q} . The inclusion of more complex relationships likely does not affect our model's qualitative results, as most latitudinal distribution models also peak at the equator and dissipate towards the poles. In addition, the shape of these distribution shifts wildly as the climate warms and is difficult to track without GCMs [30].

Thus the planet-integrated weathering flux (in mol SiO_2/yr) at any given time t is given by

$$W_{\text{SiO}_2}(t) = \frac{A_{\text{land}}}{n_{\text{grid}}} \sum_{i=1}^{n_{\text{grid}}} W_i(T_{s,i}, k_{\text{eff}}(T), q_i(T, \Phi_i)), \quad (3.6)$$

where A_{land} is the total land area and n_{grid} is the total number of grid points. T_s , T , and Φ are also functions of t for each grid point. A distinction should be made between the terms **weathering flux**, described by Equation 3.6 and **weatherability**, which we define as the weathering flux at any *given* values of pCO_2 , and T (typically $\text{pCO}_2 = 400 \times 10^{-6}$ bar, $T = 288$ K). **Weatherability** does not take into account the time evolution of the climate given imbalances in weathering and outgassing. A planet with a larger fraction of colliding area may have a lower weathering flux at low temperatures than one with a low fraction of colliding area at high temperatures, but will have a higher weatherability. An example plate collision and its effect on weatherability can be seen in Figure 3.2.

3.3 SiO_2 fluxes and CO_2 Consumption

The amount of CO_2 sequestered from the atmosphere due the dissolution of silicate rocks is not a molar one to one ratio as suggested by Reactions 2.1 and 2.2. This can be attributed to different types of silicates leading to different reaction stoichiometries, as well as the efficiency of the reactions themselves. In order to relate the

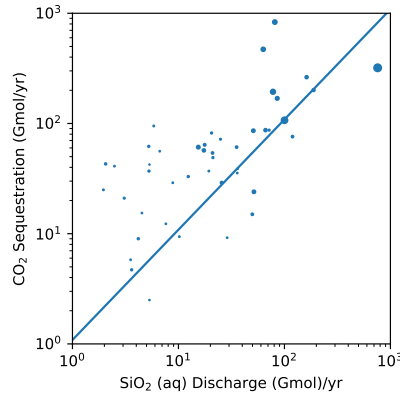


FIGURE 3.3: Silicon discharge rates and carbon consumption rates associated with various rivers presented in Gaillardet et al. [8]. Size of each point represents the total discharge of dissolved solids and associated weights for each river in our slope determination. The line represents a linear relationship of slope 1.087.

SiO_2 fluxes calculated in Equation 3.6 to the effect on atmospheric CO_2 consumption, we interpolate the results of Gaillardet et al. [8], who measured the concentrations of various dissolved solids (including Ca^{2+} , Mg^{2+} , HCO_3^- , and SiO_2) and discharge rates attributed to 60 of the largest rivers in the world. They also estimated the atmospheric CO_2 consumption from silicate weathering for each river based on various ion discharge fluxes. We ignore data from 11 rivers that are presented as highly-polluted from anthropogenic waste. By weighing the CO_2/SiO_2 ratio of each river by its total annual discharge of dissolved solids, we calculate an average molar CO_2/SiO_2 ratio of 1.087—for every mole of SiO_2 weathered and flushed out to the ocean, 1.087 moles of CO_2 are removed from atmosphere. Raw data and the line of best fit can be seen in Figure 3.3. Thus, the global CO_2 drawdown flux (in mol CO_2/yr) in our model is

$$W_{\text{CO}_2}(t) = 1.087W_{\text{SiO}_2}(t). \quad (3.7)$$

3.4 Time Evolution

The model calculates the volcanic outgassing flux of CO_2 F_{vol} by assuming that outgassing and silicate weathering are initially in a steady state:

$$F_{\text{vol}} = W_{\text{CO}_2}(t = 0). \quad (3.8)$$

This leads to different outgassing fluxes for different continental configurations, with generally higher values of F_{vol} for setups with initially colliding plates. Outgassing flux remains constant throughout each simulation run. Initial pCO_2 and temperature conditions are chosen to mimic that of present-day Earth [$\text{pCO}_2(t = 0) = 400 \times 10^{-6}$ bar, $T(t = 0) = 288$ K]. Temperature is calculated as a function of pCO_2 , explained in-detail in Appendix A.1.

Disk locations, global weathering fluxes, ocean and atmospheric carbon reservoir content, temperature, and ocean pH are all calculated in adjustable time steps. We use a time step $dt \gg 1000$ years so that the ocean and atmosphere equilibriate without consideration of short-term disequilibrium effects (i.e. Archer, Kheshgi, and

Maier-Reimer [1]). Changes in the total inorganic carbon reservoir are calculated per time step as

$$\frac{\Delta C(t)}{dt} = W_{\text{CO}_2}(t) - F_{\text{vol}}. \quad (3.9)$$

We then calculate the effects of ΔC on ocean-atmosphere partitioning, described in Appendix A.2. Thus, at each time step we record the global variables time t , globally integrated CO_2 drawdown weathering flux, $p\text{CO}_2$, ocean dissolved inorganic carbon content, globally averaged surface temperature T , and disk/point locations.

3.5 Climate Catastrophes

In order to study the overall climate stability of a given setup, we monitor two possible ‘catastrophes’—the runaway greenhouse effect and snowball events. While these events may not spell the end of life as we know it, they would almost certainly lead to mass extinctions of unprecedented scale.

3.5.1 Runaway Greenhouse

The runaway greenhouse effect occurs when greenhouses gas concentrations are high enough to prevent OLR emitted by Earth from cooling the planet. This can also be triggered by an increase in ISR. Venus may have had liquid water on its surface before experiencing a runaway greenhouse and Earth will inevitably experience one as the Sun becomes more luminous [21]. How much atmospheric CO_2 levels would need to increase in order to trigger a runaway greenhouse has been an area of active research due to rising anthropogenic emissions, with varying results based on prior assumptions.

We use results from Ramirez et al. [32], who found that a runaway greenhouse effect could occur on Earth for $p\text{CO}_2 \gtrsim 5000 \times 10^{-6}$ bar. Their study notes that this is likely the worst-case scenario, as they claim that their assumptions about H_2O absorption coefficients and how relative humidity changes with temperature use the ‘most alarmist’ parameters possible (for example, previous studies have allowed for CO_2 concentrations up to 30000×10^{-6} bar before a runaway [12]). Nevertheless, their study provides us with an approximate threshold for a ‘climate catastrophe’ end case for our simulations.

3.5.2 Snowball events

Snowball events occur when the entirety of Earth’s oceans become frozen over at the surface. This can occur when greenhouse gas concentrations become low enough to trigger a runaway ice-albedo feedback. Water ice reflects a much larger portion ($A \sim 0.6$) of ISR compared to land ($A \sim 0.3$) or open oceans ($A \sim 0.1$) [15, 20]. When the climate cools and polar ice begins to form, less ISR reaches Earth’s surface, further cooling the planet and causing more ice to form, which can eventually lead to total glaciation of the surface. Evidence has shown that Earth has been able to escape such snowball states [23]; frozen land causes weathering to decrease drastically, allowing for the gradual buildup of atmospheric CO_2 via volcanism, eventually warming the planet enough to melt the ice. However, if temperature and pressure conditions at the poles become cold enough for gaseous CO_2 to condense into solid form, the planet would likely enter an inescapable snowball state [31].

In our simulations, we treat the snowball case as a second ‘climate catastrophe’. While the Earth has likely survived at least two clusters of snowball events, including these events helps us better represent the **overall** climate stability of varying tectonic setups. In addition, modeling exactly *how* the climate escapes a Snowball Earth episode is still an active area of research [20]. We use a minimum globally average surface temperature of $T_{min} = -10^{\circ}\text{C}$ to prescribe when the surface would be cold enough to likely trigger a runaway ice-albedo feedback and subsequent snowball event. Several studies have used the local temperature $T \sim -10^{\circ}\text{C}$ as the boundary where local oceans completely freeze over [20].

3.6 Non-Tectonic Weathering Processes

On modern Earth, there are several weathering reactions that contribute to CO_2 drawdown that are independent of processes modelled in Maher and Chamberlain [28] and are thus difficult to include in our idealized model.

3.6.1 Seafloor Weathering

These effects most notable includes seafloor weathering, which occurs when seawater reacts with upper-layer oceanic crust basalts to release soluble cations. Calcium cations are then able to reaction with bicarbonate ion via Reaction 2.2 to remove a two molecules of inorganic carbon from the ocean-atmosphere system. Seafloor weathering is generally thought to display a similar dependence on surface temperature with a weak dependence on pCO_2 [37], and may be important in climate regulation of water worlds, theorized exoplanets that contain enough water to drown out any land at the surface [24]. On modern Earth, carbon drawdown from seafloor weathering is $\sim 8 - 28\%$ of that of silicate weathering [27].

3.6.2 Dust Transport

A large portion (possibly up to $\sim 10\%$ in some regions [18]) of modern-day silicate weathering is controlled by the import of exogenic dust, or mineral aerosols, mixed into the upper layer of the weathering zone. Circulation of dust by wind can inflate the amount of weathering minerals available in tectonically dead regions. Exact weathering fluxes due to dust are difficult to constrain as they require precise knowledge of dust production and climate circulation patterns.

3.6.3 Physical Erosion and Glaciers

Physical erosion (the removal of materials from the surface) naturally resupplies tectonically inactive areas with fresh minerals assuming a non-zero weathering zone thickness. Erosion of the upper layer of the weathering zone causes the zone to gradually approach the underlying bedrock, exposing it to fresh minerals. Physical erosion rates vary across the globe and are closely linked to tectonic uplift and the amount of precipitation received. Rates on Earth can vary from $4 \mu\text{m}/\text{yr}$ in tectonically inactive regions like Sri Lanka to $3000 \mu\text{m}/\text{yr}$ in the Himalayas [14] and are represented in the MaC model by the soil residence time T_s .

Evidence has shown that the presence of glaciers increase local rates of physical erosion [34], which decreases effective T_s , increasing weathering rates for a given precipitation. Thus, tracking glacier movement over glacial-interglacial cycles when

Earth is in an icehouse state is important in determining precise values for T_s , but impossible in an idealized model.

3.6.4 A Maximum Effective Soil Age $T_{s,max}$

The above processes are difficult, if not impossible, to keep track of in an idealized model. We represent these process through a maximum effective soil age $T_{s,max}$, so that soils never become completely leached of weathering minerals. We solve for this age by fitting D_w to the 'global minimum' value of 0.003 cited in Maher and Chamberlain [28], corresponding to the approximate lowest value observed through field measurements. This leads to a value of $T_{s,max} \approx 700000$ years.

Chapter 4

Results

4.1 Trial Parameters

We aim to track the effects of both overall land area coverage and number of plates on climate stability. We vary total land area as $A_{\oplus}/10$, $A_{\oplus}/3$, and A_{\oplus} , where $A_{\oplus} = 1.49 \times 10^{14} \text{ m}^2$, approximating Earth’s modern day land-coverage. We vary the number of plates as 2, 4, and 8. We use land area and number of plates to define a 9-member grid of scenarios. The $A = A_{\oplus}, N = 8$ scenario represent the ‘Earth-like’ base case.

We track the evolution of these 9 tectonic setups over a timescale of 500 million years. While this timescale is much shorter than the duration that life has existed on Earth ($\gtrsim 3.465 \text{ Gy}$ according to Schopf et al. [36]), the timescale is similar to the length of the current Phanerozoic Eon ($\sim 541 \text{ My}$), where the majority of the evolution of complex life has occurred and thus is relevant to the ultimate emergence of intelligent life. We run each scenario for 65 trials, for a total of $2 \times 9 \times 65 = 1170$ model runs. Example model runs resulting in runaway greenhouses, snowball events, and neither (survival) can be seen in Figures 4.1, 4.2, and 4.3. Climate catastrophes in our simulations are terminal and thus runaway greenhouses and snowball events are mutual exclusive.

4.2 No $T_{s,max}$ Case

In this case, we set the initial soil age of all non-colliding grid points to $T_s = 100 \text{ My}$. Soils are allowed to age to infinity, but are reset to $T_s = T_{reset}$ when colliding. This simulates the behavior we would expect if (a) CO_2 drawdown was only regulated by silicate weathering and (b) only tectonic collisions supplied fresh minerals for weathering. Results can be seen in Figure 4.4. Survival rates for all scenarios are generally low, with an average survival rate of 33%.

4.3 $T_{s,max}$ Case

In this case, soils are allowed to age to a maximum effective age $T_{s,max}$, described in Section 3.6.4. Results can be seen in Figure 4.5. Survival rates are noticeably higher than the no $T_{s,max}$ case, with an average survival rate of 44%. Difference between survival rates can be seen in Figure 4.6.

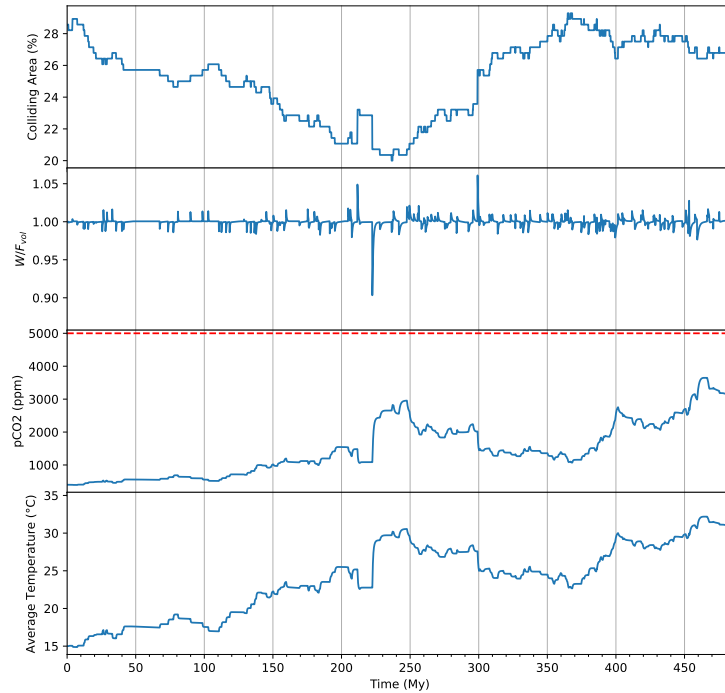


FIGURE 4.1: An example model run for an Earth-like continental plate configuration ($A = A_{\oplus}, N = 7$ with $T_{s,max}$) ending in a runaway greenhouse after 485 My. ‘Colliding Area’ represents the amount of grid points that are colliding at any given time divided by the total number of grid points. Spikes in the weathering-to-outgassing ratio W/F_{vol} are caused by the change in the area of mountain belts due to plate collisions and separations. The climate is generally stable for the first 150 My, after which a gradual decrease of collisional area causes pCO_2 and global temperatures to rise, lowering the feedback strength of silicate weathering and causing it to be more susceptible to changes in W (see Appendix A.3 for a derivation of feedback strength as a function of temperature).

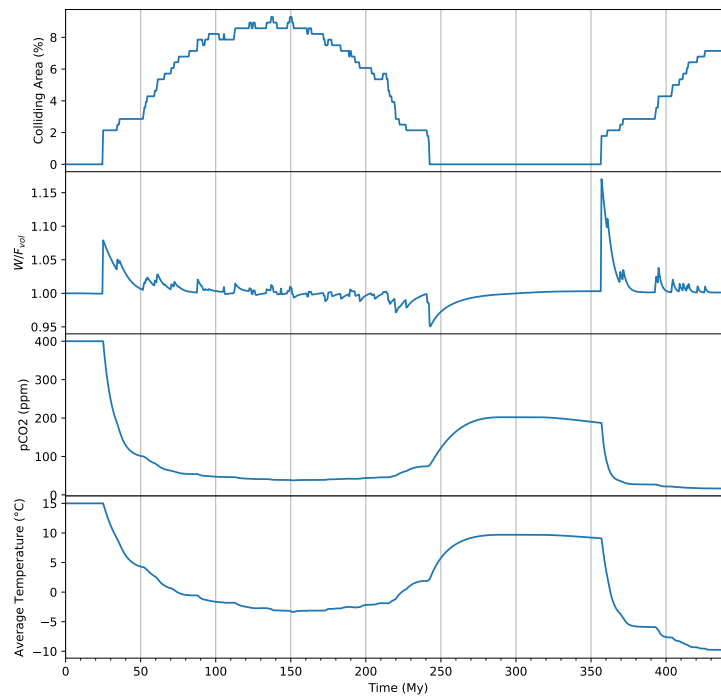


FIGURE 4.2: An example model run for planet with a low land coverage ($A = A_{\oplus}/3, N = 7$ with $T_{s,max}$) ending in a snowball state after 485 My. An initial colliding area of 0 leads to a low initial weathering rate and outgassing flux F_{vol} . The low value of F_{vol} in this model run causes the planet to become more susceptible to transient collisions, which increase local weatherability by a factor of 20.

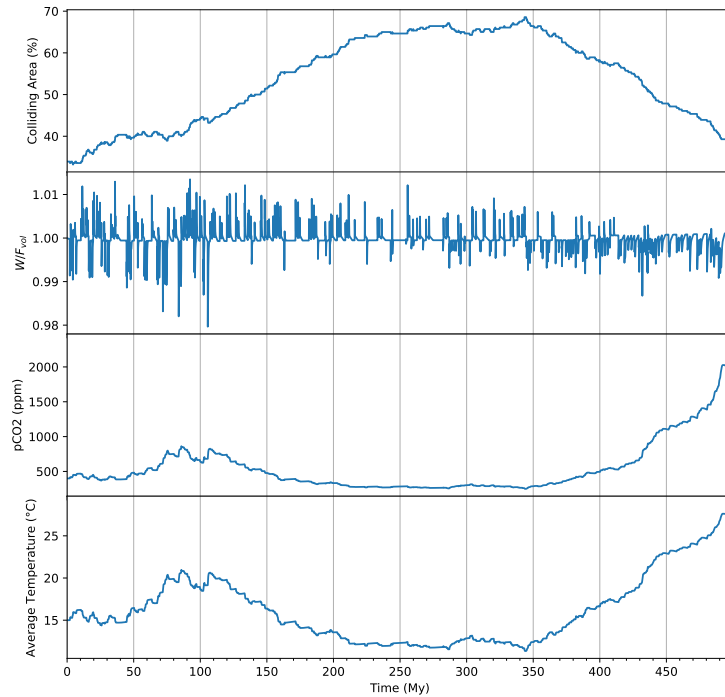


FIGURE 4.3: An example model run for an Earth-like continental plate configuration ($A = A_{\oplus}, N = 7$ with $T_{s,max}$) that remains stable despite a $\sim 2\times$ increase in colliding area, mimicking the formation of a supercontinent. An initial gradual increase in the amount of mountain belts causes imbalances in weathering and outgassing that decrease global temperatures, thereby decreasing precipitation rates and rebalancing CO_2 fluxes. A detaching of collision zones around ~ 350 Myr cause global temperatures to steadily rise as weatherability of the planet decreases.

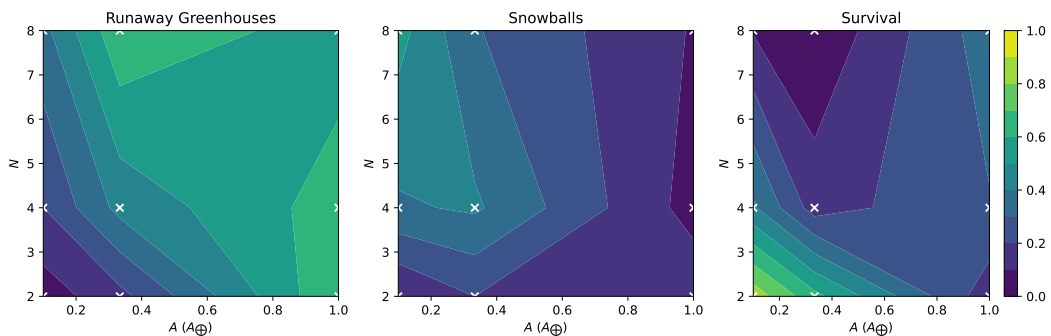


FIGURE 4.4: Climate catastrophe and survival rates for the no $T_{s,max}$ case. White crosses indicate the scenarios sampled. High survival rates tend to cluster around very low A, N cases but generally increase with high A, N . Survival rate for the Earth-like base case ($A = A_{\oplus}, N = 8$) is 35%.

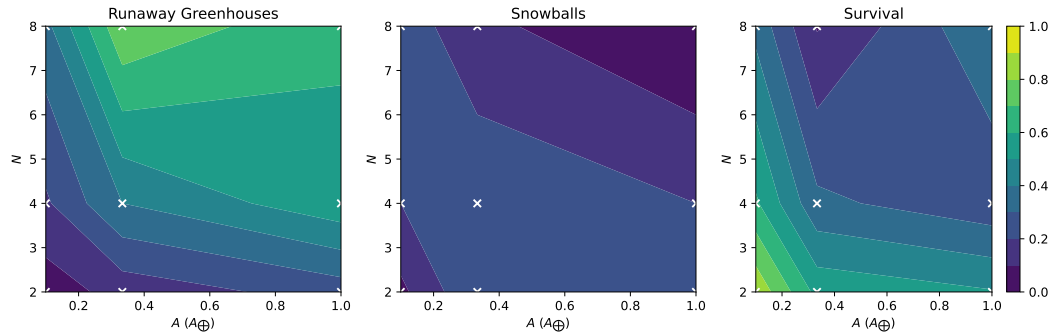


FIGURE 4.5: Climate catastrophe and survival rates for the $T_{s,max}$ case. Survival rate for the Earth-like base case ($A = A_{\oplus}, N = 8$) is 37%.

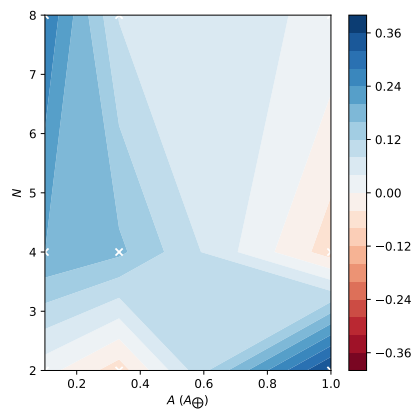


FIGURE 4.6: Difference of survival rates in the $T_{s,max}$ and no $T_{s,max}$ cases. Including $T_{s,max}$ improves survival rates in 7/9 scenarios—displaying a maximum improvement in survival rate of 37% in the $A = A_{\oplus}, N = 2$ case and a maximum deficit in the $A = A_{\oplus}/3, N = 2$ case of 6%.

4.4 Model Biases

Survival in our model is naturally biased towards cases with low outgassing flux that never experience plate collisions (‘no collision cases’). This is most notable in the $A = A_{\oplus}/10, N = 2$ cases which rarely ever experience a single collision. A lack of initial colliding area cause initial weathering fluxes and thus F_{vol} values to be extremely low (down to $\sim 10^{-4}F_{\oplus}$ in no $T_{s,max}$ cases, where $F_{\oplus} = 0.085$ GtC/yr [27]). Low F_{vol} values prevent runaway greenhouses on 500 My timescales since, even with a weathering drawdown flux of $W_{CO_2} = 0$, outgassing alone is unable to reach pCO₂ levels $> 5000 \times 10^{-6}$ bar. This is especially true in the $T_{s,max}$ case, as weathering fluxes stay roughly constant in no collision cases instead of asymptotically decreasing towards 0 as soil ages indefinitely. Even if $W_{CO_2} = 0$, low outgassing fluxes in many simulations would take $\gg 500$ My to build up the present-day 35600 gigatonnes of carbon (GtC) atmosphere/ocean carbon reservoir, in what can be thought of as the ‘carbon build-up timescale’, distinct from the carbon residence timescale:

$$\tau_C = \frac{35600 \text{ GtC}}{F_{vol}}. \quad (4.1)$$

For Earth, $\tau_C \sim 400$ ky, but this timescale increases in many of the no collision cases ($F_{vol} \sim 10^{-4}F_{\oplus} \rightarrow \tau_C \sim 4$ By). Simulating each scenario for a similar multiple of τ_C would thus be more representative of the scenario’s actual long-term stability.

This, however, is not the case for snowball events, which can occur at any outgassing flux. At low latitudes, collisions increase the local weatherability by a factor of 20, assuming initial soil age $T_s = T_{s,max}$. Scenarios that begin with no initial collisions and only experience sporadic collisions are susceptible to large imbalances in weathering and outgassing. Migration of continents into low-latitude zones with higher precipitation can also increase global weathering. This effect is more prominent in colliding regions, where weathering flux increases by a factor of 1.8 moving from high ($\Phi = 60^\circ$) to low ($\Phi = 0^\circ$) latitudes. Weathering in old soils ($T_s = T_{s,max}$) only increases across these latitudes by a factor of 1.04. Susceptibility to climate catastrophes as a function of F_{vol} and collision frequency can be seen in Figures 4.7 and 4.8.

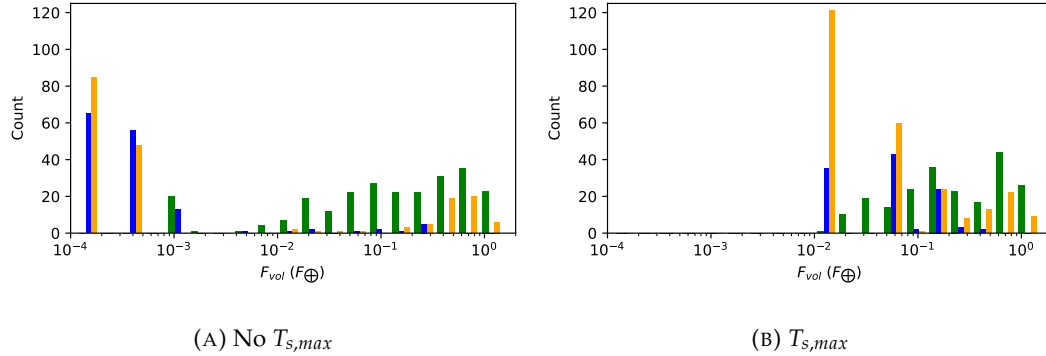


FIGURE 4.7: Number of climate catastrophe (runaway greenhouses in green, snowball events in blue) and survival cases (orange) as a function of volcanic outgassing F_{vol} normalized to present-day estimates for Earth’s outgassing flux ($F_{\oplus} \sim 0.085$ GtC/yr [27]). No collision survival bias towards low F_{vol} , discussed in Section 4.4, is clearly visible in the no $T_{s,max}$ case for $F_{vol} \lesssim 10^{-3}F_{\oplus}$. At outgassing fluxes past this regime, survival rates generally increase with F_{vol} . The number of snowball events tend to decrease drastically for large F_{vol} values in both cases ($F_{vol} \gtrsim 2 \times 10^{-3}F_{\oplus}$ for no $T_{s,max}$ cases, $\gtrsim 2 \times 10^{-1}F_{\oplus}$ for $T_{s,max}$ cases) as susceptibility to runaway greenhouses increases.

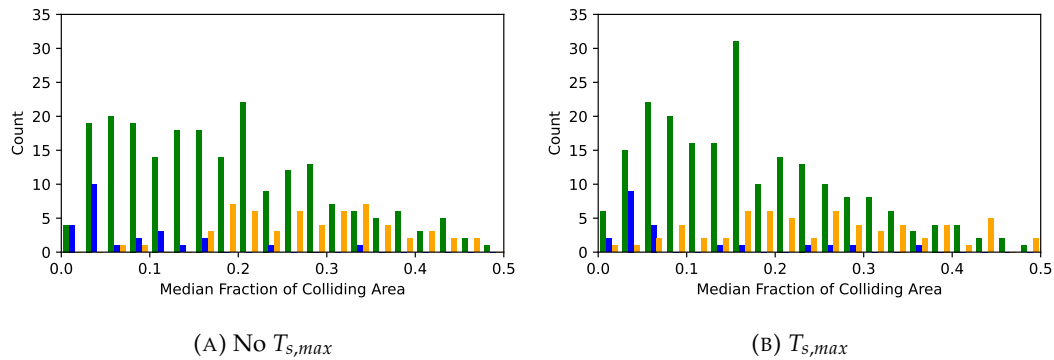


FIGURE 4.8: Number of climate catastrophe (runaway greenhouses in green, snowball events in blue) and survival cases (orange) as a function of the median fraction of colliding land area in each simulation, excluding ‘no collision’ cases (median fraction= 0) to reduce low F_{vol} /no collision survival bias. Both cases suggest a increased average survival rate for cases with more frequent collisions.

Chapter 5

Conclusion

Our model results demonstrate that the climate stability of planets with Earth-like plate tectonics and ocean content benefits from higher numbers and area of continental plates as well as more frequent continental plate collisions. Including the effect of weathering processes not associated tectonic collisions through the introduction of $T_{s,max}$ increases overall survival rate by 33%, although these planets are still susceptible to climate catastrophes.

We also showed that our idealized model shows a high survival-rate bias towards planets with low volcanic outgassing fluxes on timescales less than the build-up timescale of Earth’s ocean/atmosphere carbon reservoir. Regardless of model biases, a higher number of trials per scenario is required to accurately assess statistics. Increasing the sample space of our A, N grid (particularly for $A > A_{\oplus}$ or $N > 8$ cases) will also help in our understanding of how stability explicitly relies on F_{vol} , A , and N . Our preliminary results suggest that frequent collisions and higher outgassing fluxes, which both typically occur at higher values of A and N , are conducive to long-term climate stability.

5.1 Model Limitations and Future Work

Many complexities of the modern-day silicate-carbonate weathering feedback on Earth are ignored in our model for the sake of simplicity. Like all Earth systems, the realities of the carbonate-silicate weathering feedback are incalculably complex and intertwined with a variety of other systems that have their own time-evolution. However, the following additions could conceivably be taken into account in future versions of DISKWORLD.

5.1.1 Ice Albedo Feedback and $T(pCO_2)$

Our global temperature’s dependence on pCO_2 presented in Appendix A.1 is overly simplified and does not include many basic systems that govern Earth’s climate. In future iterations, we plan on adding ice-albedo feedback effects using methods presented in Kadoya and Tajika [20], who used a new formulation for albedo of an icehouse planet alongside OLR interpolations of simulation data presented in Kopparapu et al. [25], to our pCO_2 -temperature curves to better model exactly when snowball events occur.

5.1.2 Precipitation and Runoff

In addition to effects outlined in Section 3.2, distance from the ocean also greatly affects how much precipitation is received inland as it becomes more difficult to transport water vapor originating from the ocean over long stretches of land [16]. River

runoff is also required to travel long distances to the ocean without being evaporated first. Distance from the ocean could thus also be a variable included in Equation 3.1.

5.2 Paleoreconstructions

Given paleodata of localized precipitation/runoff, surface temperatures, and continental plate topography, our model could be used to determine paleo-pCO₂ concentrations similar to analyses performed with the GEOCARB and GEOCLIM climate models [2, 7, 10, 11]. This could also help assess the validity of our model if we are able to reproduce temperatures and pCO₂ levels calculated from proxies. This would require a more accurate determination of the weathering-zone/soil thickness L and the effective soil age T_s , which are functions of the physical erosion rate E and rate of regolith production, as well as the inclusion of non-tectonic weathering processes.

Appendix A

Appendix

TABLE A.1: Definition of select model parameters with units and formulae where applicable. For a more detailed table of weathering flux-related parameters, see the supplemental material of Maher and Chamberlain [28].

Parameter	Definition	Units	Value
R_p	Planetary Radius	m	6.371×10^6
ISR	Solar Insolation Flux	W/m^2	1361
$p\text{CO}_{2,0}$	Initial Atmospheric CO2 Concentration	bar	400×10^{-6}
T_0	Initial Globally-Averaged Surface Air Temperature	K (°C)	288 (15)
C_{ocean}	Initial Ocean Inorganic Carbon Reservoir	GtC	35000
V_{ocean}	Ocean Volume	L	1.37×10^{21}
\bar{p}_{ref}	Modern Global Average Precipitation	m/yr	1.0 [45]
Γ	Runoff Coefficient		0.259 [9]
L	Reactive Flow Path Length	m	1
ϕ	Soil Porosity		0.175
ρ_{sf}	Mineral Mass to Fluid Volume Ratio	g/L	12728
A	Specific Surface Area	m^2/g	0.1
X_r	Reactive Mineral Concentration in Fresh rock		0.36
m	Molar Mass of Weathering Minerals	g/mol	270
k_{eff}	Reference Rate Constant	$\text{mol}/\text{m}^2/\text{yr}$	8.7×10^{-6}
E_a	Silicate Weathering Activation Energy	kJ	38
$T_{s,reset}$	Soil Age During a Collision	yr	2888
$T_{s,startup}$	Model Start-up Time	yr	10^8
$T_{s,max}$	Maximum Effective Soil Age	yr	704798
R	Disk Radius	m	Variable, default 2.6×10^7
N	Number of Disks		Variable, default 7
V	Average Disk Velocity	m/yr	0.10
σ	Disk Velocity Standard Deviation	m/yr	0.05
γ	Land fraction		$NR^2/(4R_p^2)$

A.1 $p\text{CO}_2$ and Global Temperatures

Several studies have modeled the effect of $p\text{CO}_2$ on global average temperatures as the results are relevant to both modern-day anthropogenic carbon emissions and atmospheric compositions of terrestrial exoplanets. We use a simplified log-linear relationship based on results presented in Wordsworth and Pierrehumbert [43]. They calculated the effects of increasing $p\text{CO}_2$ ($10^{-4} - 50$ bar) and T_{surf} (250 – 500 K) in a pure $\text{N}_2 - \text{CO}_2 - \text{H}_2\text{O}$ atmosphere, assuming full saturation of H_2O , on OLR and planetary albedo. We interpolate their results to solve for the steady state solution,

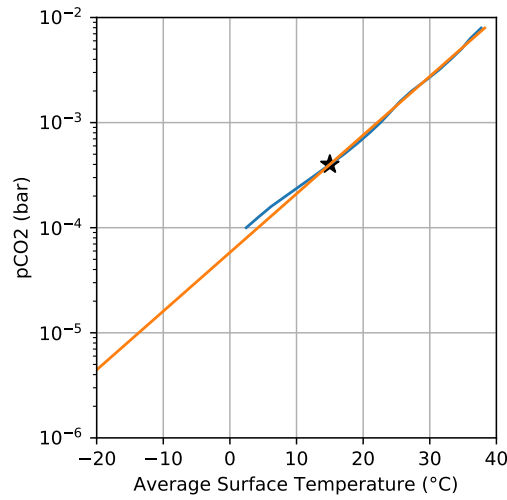


FIGURE A.1: Log-linear temperature fits used in our model and described in Equation A.3 (orange) alongside interpolated data from Wordsworth and Pierrehumbert [43] (blue). The star represents modern-day Earth conditions ($T = 15^\circ\text{C}$, $p\text{CO}_2 = 400 \times 10^{-6}$ bar).

$$\text{OLR}(T, p\text{CO}_2) = (1 - \alpha(T, p\text{CO}_2)) \frac{\text{ISR}}{4}, \quad (\text{A.1})$$

assuming $\text{ISR} = 1361 \text{ W/m}^2$. This gives us a solution for the steady state $T(p\text{CO}_2)$, which we then fit for a log-linear relationship via linear regression. The interpolations overestimate Earth's current average surface temperature ($\sim 15^\circ\text{C}$) by about 19.6°C , likely due to assuming water vapor saturation. We apply a constant subtraction of $\Delta T = 19.6 \text{ K}$ to mimic present-day Earth conditions, giving us

$$T \approx 348.84 + 7.776 \ln(p\text{CO}_2), \quad (\text{A.2})$$

where T is in units of K and $p\text{CO}_2$ is in bars, or

$$T \approx 15 + 7.776 \ln\left(\frac{p\text{CO}_2}{400 \text{ ppm}}\right) \quad (\text{A.3})$$

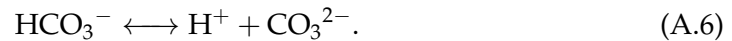
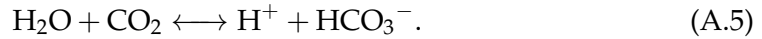
where T is in units of $^\circ\text{C}$. Interpolation data and the fitted regression line can be seen in Figure A.1.

This relationship implies a global climate sensitivity of $\Delta T(2\times) = 7.776 \ln(2) = 5.4 \text{ K}$ per doubling of $p\text{CO}_2$. In reality, climate sensitivity is a complex function a myriad of factors including global precipitation rates, continental configuration, and ocean heat transport and has varied over Earth's history. Royer, Berner, and Park [35] calculated 5 – 95% confidence intervals of $\Delta T(2\times) = 1.5 - 6.2 \text{ K}$ for the Phanerozoic Eon based on proxies for $p\text{CO}_2$ and temperature. Our estimate is notably close to the results of Krissansen-Totton and Catling [26], who calculated $\Delta T(2\times) = 5.6 \text{ K}$ based on the strength of the carbonate-silicate weathering feedback on modern-day Earth.

Interpolation of the results of Wordsworth and Pierrehumbert [43] also leads to a vanishing of steady-state results for $p\text{CO}_2 > 0.01$ bar, implying a runaway greenhouse at $p\text{CO}_2 \approx 9900$ ppm for their model.

A.2 CO₂ Partitioning and Ocean Chemistry

To calculate partitioning of inorganic carbon within the ocean and atmosphere, we use the software package *csys* [48], which calculates various equilibrium constants pertaining to ocean chemistry. Dissolved inorganic carbon (DIC) is partitioned in the ocean between various aqueous species, namely H₂CO₃/CO₂ (aq), HCO₃⁻, and CO₃²⁻. The amount of each species is governed by the following reactions:



The equilibrium constants for each of the above reactions (commonly referred to as K_H , K_1 , and K_2 , respectively) are functions of ocean temperature, salinity, and atmospheric pressure. *csys* uses equations for each equilibrium constant based on high-precision measurements with seawater.

It is important to keep track of ocean chemistry since as carbon is added to the ocean-atmosphere system, the ocean becomes more acidic and the fraction of carbon stored in the atmosphere versus ocean increases (see Appendix A of Wordsworth and Pierrehumbert [43] for an example). Ocean surface temperature also affects the ability of CO₂ to be dissolved in the ocean, with higher temperatures increasing the relative amount of carbon stored in the atmosphere. For these reasons, in addition to pCO₂, the amount of DIC stored in the ocean, C_{ocean} , and the pH of the ocean are kept track of in our simulations.

Calculating the partitioning of CO₂ between the atmosphere and ocean heavily relies on the concept of alkalinity, which is defined as the difference in charge of conservative ions and has units of equivalent charge per liter or kilogram of water. Conservative ions are dissolved solids that are generally unaffected by changes in temperature, salinity, and pressure, e.g. Na⁺, Ca²⁺, Cl⁻, and SO₄²⁻. Given that the ocean is charge neutral on a global scale, non-conservative ions (ions sensitive to temperature, salinity, and pressure changes e.g. HCO₃⁻, CO₃²⁻, B(OH)₄⁻, and H⁺) are required to counteract charge imbalances. In seawater, DIC represents the vast majority of non-conservative ions, and the alkalinity can be approximated as the **carbonate alkalinity**, defined as

$$\text{ALK} \approx [\text{HCO}_3^-] + 2[\text{CO}_3^{2-}]. \quad (\text{A.7})$$

The addition or removal of CO₂ to the ocean-atmosphere system does not affect the alkalinity on timescales longer than the calcium carbonate compensation time ($\sim 10^4$ yr)—alkalinity increases from the introduction of conservative cations (Ca²⁺) in Reaction 2.1 are balanced by the calcite precipitation in Reaction 2.2, and thus there is no net change in the system alkalinity [47, 5]. Thus, we can solve for ocean-atmosphere carbon partitioning by keeping alkalinity constant and adjusting pCO₂ until the total carbon content is consistent with the perturbation. The carbonate alkalinity of the ocean given our starting assumptions is 2.36 mEq/L, in line with modern estimates of 2.3 – 2.5 mEq/L [33]. An example of the long-term response of our ocean-atmosphere system to a perturbation in carbon content can be seen in Figure A.2.

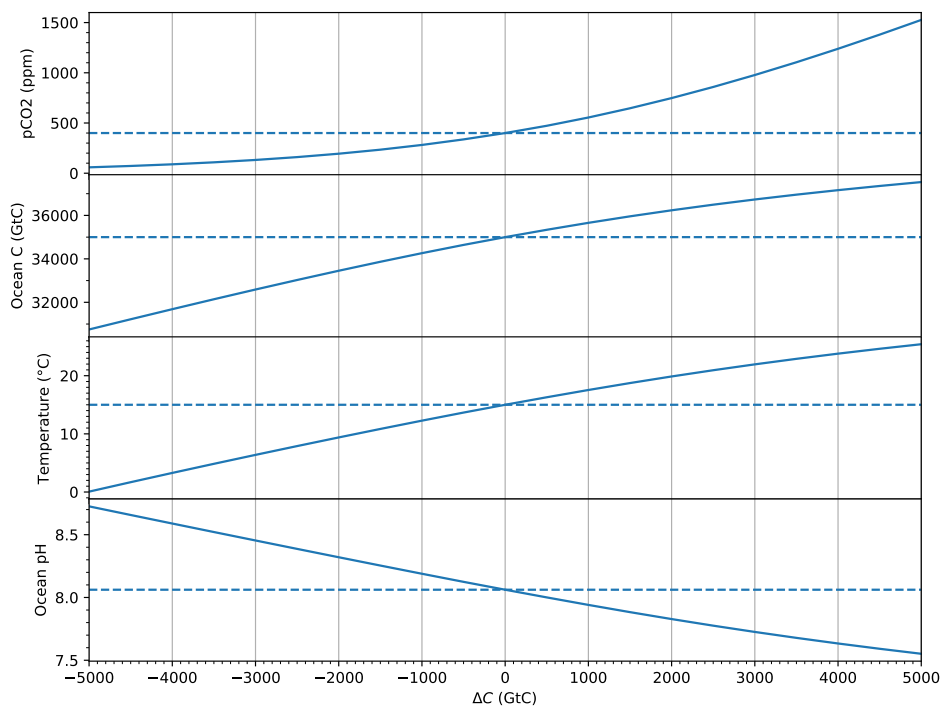


FIGURE A.2: Response of atmospheric/ocean CO₂ content, globally average surface temperature, and ocean pH to carbon perturbations up to 5000 GtC, about 14% of the current ocean-atmosphere reservoir, based on methods outlined in Appendix A.2. Dashed lines represent initial conditions of our model. The ocean becomes notably less receptive to the addition of carbon as more is added to the system.

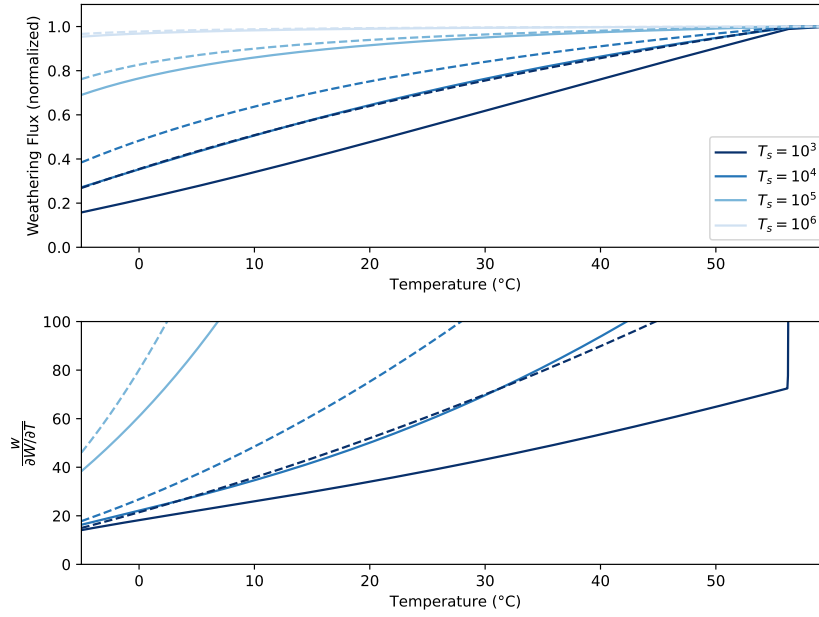


FIGURE A.3: (Top) Weathering flux as a function of temperature for various soil ages in years (T_s), normalized to their individual maxima. Solid lines include the temperature dependencies of Equation A.8, while dashed lines do not. (Bottom) The temperature change required to rebalance a 100% increase or decrease in global weathering at a given soil age, assuming that precipitation increases linearly with temperature. Lower values represent more stable climates. The sharp increase at $T = 55^\circ\text{C}$ represents when the system reaches precipitation saturation, $\bar{p} = \bar{p}_{max}$, as described in Equation 3.3.

A.3 MaC Model Temperature and pCO_2 Dependencies

While temperature dependencies of the reactions governing weathering were ignored in Maher and Chamberlain [28], we find that their inclusion significantly alters the strength of the global weathering feedback.

Similar to the WHaK model, k_{eff} has a weak dependence on temperature and the partial pressure of CO_2 , pCO_2 , defined by the Arrhenius relationship:

$$\frac{k_{eff}(T)}{k_{eff}(T_0)} = e^{\frac{E_a}{R}(\frac{1}{T_0} - \frac{1}{T})} \left(\frac{\text{pCO}_2}{\text{pCO}_{2,ref}} \right)^\beta, \quad (\text{A.8})$$

where E_a is the apparent activation energy of mineral dissolution and R is the gas constant. Since k_{eff} appears in both the numerator and denominator of Equation 2.5, Maher and Chamberlain [28] argue in their Supplementary Material that temperature effects are negligible. However, we find that systems including these temperature dependencies are more resilient to changes in weathering flux, shown in Figure A.3. Thus, we include the temperature and pCO_2 dependencies of k_{eff} in our model.

Winnick and Maher [42] found that C_{eq} should also exhibit a weak dependence on pCO_2 . However, they demonstrated that for low values of pCO_2 ($\lesssim 0.1$ bar) that this behavior is negligible. While study focuses on planets with Earth-like solar insolation, where the runaway greenhouse effect would occur at pressures $\text{pCO}_2 \ll 0.1$ bar, this pressure dependence could be included in future work on planets with different stellar insolation.

Bibliography

- [1] David Archer, Haroon Kheshgi, and Ernst Maier-Reimer. “Multiple timescales for neutralization of fossil fuel CO₂”. In: *Geophysical Research Letters* 24.4 (1997), pp. 405–408. DOI: [10.1029/97GL00168](https://doi.org/10.1029/97GL00168).
- [2] Robert A. Berner. “GEOCARBSULF: a combined model for Phanerozoic atmospheric O₂ and CO₂”. In: *Geochimica et Cosmochimica Acta* 70.23 (2006), pp. 5653–5664.
- [3] Donald Frederick Boucher and George E Alves. *Dimensionless Numbers: For Fluid Mechanics Heat Transfer, Mass Transfer and Chemical Reaction*. American Institute of Chemical Engineers, 1963.
- [4] Gabriel Bowen et al. “Two massive, rapid releases of carbon during the onset of the Palaeocene-Eocene thermal maximum”. In: *Nature Geoscience Online* (Dec. 2014). DOI: [10.1038/ngeo2316](https://doi.org/10.1038/ngeo2316).
- [5] Aaron Bufe et al. “Co-variation of silicate, carbonate and sulfide weathering drives CO₂ release with erosion”. In: *Nature Geoscience* 14 (Apr. 2021), pp. 211–216. DOI: [10.1038/s41561-021-00714-3](https://doi.org/10.1038/s41561-021-00714-3).
- [6] Grant M. Cox et al. “Continental flood basalt weathering as a trigger for Neoproterozoic Snowball Earth”. In: *Earth and Planetary Science Letters* 446 (2016), pp. 89–99. ISSN: 0012-821X. DOI: [10.1016/j.epsl.2016.04.016](https://doi.org/10.1016/j.epsl.2016.04.016).
- [7] Yannick Donnadieu et al. “A GEOCLIM simulation of climatic and biogeochemical consequences of Pangea breakup”. In: *Geochemistry, Geophysics, Geosystems* 7.11 (2006).
- [8] J. Gaillardet et al. “Global silicate weathering and CO₂ consumption rates deduced from the chemistry of large rivers”. In: *Chemical Geology* 159.1 (1999), pp. 3–30. ISSN: 0009-2541. DOI: [10.1016/S0009-2541\(99\)00031-5](https://doi.org/10.1016/S0009-2541(99)00031-5).
- [9] Gionata Ghiggi et al. “GRUN: an observation-based global gridded runoff dataset from 1902 to 2014”. In: *Earth System Science Data* 11.4 (2019), pp. 1655–1674.
- [10] Yves Godderis and Yannick Donnadieu. “A sink- or a source-driven carbon cycle at the geological timescale? Relative importance of palaeogeography versus solid Earth degassing rate in the Phanerozoic climatic evolution”. In: *Geological Magazine* 156.2 (Dec. 2017), pp. 355–365. ISSN: 0016-7568. DOI: [10.1017/S0016756817001054](https://doi.org/10.1017/S0016756817001054).
- [11] Yves Godderis et al. “Onset and ending of the late Palaeozoic ice age triggered by tectonically paced rock weathering”. In: *Nature Geoscience* 10 (Apr. 2017). DOI: [10.1038/ngeo2931](https://doi.org/10.1038/ngeo2931).
- [12] Colin Goldblatt et al. “Corrigendum: Low simulated radiation limit for runaway greenhouse climates”. In: *Nature Geoscience* 6 (July 2013), pp. 661–667. DOI: [10.1038/ngeo1892](https://doi.org/10.1038/ngeo1892).

- [13] Robert J. Graham and Raymond T. Pierrehumbert. “Thermodynamic and Energetic Limits on Continental Silicate Weathering Strongly Impact the Climate and Habitability of Wet, Rocky Worlds”. In: *The Astrophysical Journal* (2020).
- [14] D.E. Granger. “Cosmogenic Nuclide Dating | Landscape Evolution”. In: *Encyclopedia of Quaternary Science*. Ed. by Scott A. Elias. Oxford: Elsevier, 2007, pp. 445–452. ISBN: 978-0-444-52747-9. DOI: [10.1016/B0-44-452747-8/00386-0](https://doi.org/10.1016/B0-44-452747-8/00386-0).
- [15] Jacob Haqq-Misra et al. “Limit cycles can reduce the width of the habitable zone”. In: *The Astrophysical Journal* 827.2 (2016), p. 120.
- [16] D. Hayward and Robin Clarke. “Relationship between rainfall, altitude and distance from the sea in the Freetown Peninsula, Sierra Leone”. In: *Hydrological Sciences Journal* 41 (June 1996), pp. 377–384. DOI: [10.1080/02626669609491509](https://doi.org/10.1080/02626669609491509).
- [17] B. Henderson-Sellers. “A new formula for latent heat of vaporization of water as a function of temperature”. In: *Quarterly Journal of the Royal Meteorological Society* 110.466 (1984), pp. 1186–1190. DOI: [10.1002/qj.49711046626](https://doi.org/10.1002/qj.49711046626).
- [18] George E. Hilley and Stephen Porder. “A framework for predicting global silicate weathering and CO₂ drawdown rates over geologic time-scales”. In: *Proceedings of the National Academy of Sciences* 105.44 (2008), pp. 16855–16859. DOI: [10.1073/pnas.0801462105](https://doi.org/10.1073/pnas.0801462105).
- [19] Paul F. Hoffman et al. “A Neoproterozoic Snowball Earth”. In: *Science* 281.5381 (1998), pp. 1342–1346. DOI: [10.1126/science.281.5381.1342](https://doi.org/10.1126/science.281.5381.1342).
- [20] Shintaro Kadoya and E. Tajika. “Outer Limits of the Habitable Zones in Terms of Climate Mode and Climate Evolution of Earth-like Planets”. In: *The Astrophysical Journal* 875 (Apr. 2019), p. 7. DOI: [10.3847/1538-4357/ab0aef](https://doi.org/10.3847/1538-4357/ab0aef).
- [21] James F. Kasting. “Runaway and moist greenhouse atmospheres and the evolution of Earth and Venus”. In: *Icarus* 74.3 (1988), pp. 472–494.
- [22] James F. Kasting, Daniel P. Whitmire, and Ray T. Reynolds. “Habitable Zones around Main Sequence Stars”. In: *Icarus* 101.1 (1993), pp. 108–128. ISSN: 0019-1035. DOI: [10.1006/icar.1993.1010](https://doi.org/10.1006/icar.1993.1010).
- [23] Joseph L. Kirschvink. “Late Proterozoic low-latitude global glaciation: the snowball Earth”. In: *The Proterozoic Biosphere: A Multidisciplinary Study*. Cambridge University Press, 1992. ISBN: 9780521366151.
- [24] Edwin S. Kite and Eric B. Ford. “Habitable of Exoplanet Waterworlds”. In: *The Astrophysical Journal* 864.1 (2018), p. 75. DOI: [10.3847/1538-4357/aad6e0](https://doi.org/10.3847/1538-4357/aad6e0).
- [25] Ravi Kumar Kopparapu et al. “Habitable zones around main-sequence stars: new estimates”. In: *The Astrophysical Journal* 765.2 (2013), p. 131.
- [26] Joshua Krissansen-Totton and David Catling. “Constraining climate sensitivity and continental versus seafloor weathering using an inverse geological carbon cycle model”. In: *Nature Communications* 8 (May 2017). DOI: [10.1038/ncomms15423](https://doi.org/10.1038/ncomms15423).
- [27] Cin-Ty Lee et al. “A Framework for Understanding Whole-Earth Carbon Cycling”. In: *Deep Carbon: Past to Present*. Oct. 2019, pp. 313–357. DOI: [10.1017/9781108677950.011](https://doi.org/10.1017/9781108677950.011).
- [28] K. Maher and C. P. Chamberlain. “Hydrologic Regulation of Chemical Weathering and the Geologic Carbon Cycle”. In: *Science* 343.6178 (2014), pp. 1502–1504. DOI: [10.1126/science.1250770](https://doi.org/10.1126/science.1250770).

- [29] Paul A. O’Gorman and Tapio Schneider. “The Hydrological Cycle over a Wide Range of Climates Simulated with an Idealized GCM”. In: *Journal of Climate* 21 (Aug. 2008), pp. 3815–3832. DOI: [10.1175/2007JCLI2065.1](https://doi.org/10.1175/2007JCLI2065.1).
- [30] Paul A. O’Gorman and Tapio Schneider. “Scaling of Precipitation Extremes over a Wide Range of Climates Simulated with an Idealized GCM”. In: *Journal of Climate* 22.21 (2009), pp. 5676–5685. DOI: [10.1175/2009JCLI2701.1](https://doi.org/10.1175/2009JCLI2701.1).
- [31] R.T. Pierrehumbert et al. “Climate of the Neoproterozoic”. In: *Annual Review of Earth and Planetary Sciences* 39.1 (2011), pp. 417–460. DOI: [10.1146/annurev-earth-040809-152447](https://doi.org/10.1146/annurev-earth-040809-152447).
- [32] Ramses Ramirez et al. “Can Increased Atmospheric CO₂ Levels Trigger a Runaway Greenhouse?” In: *Astrobiology* 14 (July 2014). DOI: [10.1089/ast.2014.1153](https://doi.org/10.1089/ast.2014.1153).
- [33] Phil Renforth and Gideon Henderson. “Assessing ocean alkalinity for carbon sequestration”. In: *Reviews of Geophysics* 55.3 (2017), pp. 636–674. DOI: [10.1002/2016RG000533](https://doi.org/10.1002/2016RG000533).
- [34] Clifford S Riebe, James W Kirchner, and Robert C Finkel. “Erosional and climatic effects on long-term chemical weathering rates in granitic landscapes spanning diverse climate regimes”. In: *Earth and Planetary Science Letters* 224.3-4 (2004), pp. 547–562.
- [35] Dana L. Royer, Robert A. Berner, and Jeffrey Park. “Climate sensitivity constrained by CO₂ concentrations over the past 420 million years”. In: *Nature* 446.7135 (2007), pp. 530–532.
- [36] J. William Schopf et al. “SIMS analyses of the oldest known assemblage of microfossils document their taxon-correlated carbon isotope compositions”. In: *Proceedings of the National Academy of Sciences* 115.1 (2018), pp. 53–58. DOI: [10.1073/pnas.1718063115](https://doi.org/10.1073/pnas.1718063115).
- [37] “Seafloor weathering controls on atmospheric CO₂ and global climate”. In: *Geochimica et Cosmochimica Acta* 61.5 (1997), pp. 965–973. ISSN: 0016-7037. DOI: [10.1016/S0016-7037\(96\)00385-7](https://doi.org/10.1016/S0016-7037(96)00385-7).
- [38] Ellen Thomas. “Late Cretaceous–early Eocene mass extinctions in the deep sea”. In: *Global Catastrophes in Earth History; An Interdisciplinary Conference on Impacts, Volcanism, and Mass Mortality*. Geological Society of America, Jan. 1990. ISBN: 9780813722474. DOI: [10.1130/SPE247-p481](https://doi.org/10.1130/SPE247-p481).
- [39] Toby Tyrrell. “Chance played a role in determining whether Earth stayed habitable”. In: *Communications Earth and Environment* 1.1, 61 (Dec. 2020), p. 61. DOI: [10.1038/s43247-020-00057-8](https://doi.org/10.1038/s43247-020-00057-8).
- [40] James C. G. Walker, P. B. Hays, and J. F. Kasting. “A negative feedback mechanism for the long-term stabilization of Earth’s surface temperature”. In: *Journal of Geophysical Research: Oceans* 86.C10 (1981), pp. 9776–9782. DOI: [10.1029/JC086iC10p09776](https://doi.org/10.1029/JC086iC10p09776).
- [41] Simon Wilde et al. “Evidence from detrital zircons for the existence of continental crust and oceans on the Earth 4.4 Gyr ago”. In: *Nature* 409 (Feb. 2001), pp. 175–8. DOI: [10.1038/35051550](https://doi.org/10.1038/35051550).
- [42] Matthew J. Winnick and Kate Maher. “Relationships between CO₂, thermodynamic limits on silicate weathering, and the strength of the silicate weathering feedback”. In: *Earth and Planetary Science Letters* 485 (Mar. 2018), pp. 111–120. DOI: [10.1016/j.epsl.2018.01.005](https://doi.org/10.1016/j.epsl.2018.01.005).

- [43] R. D. Wordsworth and R. T. Pierrehumbert. "Water loss from terrestrial planets with CO₂-rich atmosphere". In: 778.2 (2013), p. 154. DOI: [10.1088/0004-637x/778/2/154](https://doi.org/10.1088/0004-637x/778/2/154).
- [44] James D. Wright and Morgan F. Schaller. "Evidence for a rapid release of carbon at the Paleocene-Eocene thermal maximum". In: *Proceedings of the National Academy of Sciences* 110.40 (2013), pp. 15908–15913. DOI: [10.1073/pnas.1309188110](https://doi.org/10.1073/pnas.1309188110).
- [45] Pingping Xie and Phillip A. Arkin. "Global Precipitation: A 17-Year Monthly Analysis Based on Gauge Observations, Satellite Estimates, and Numerical Model Outputs". In: *Bulletin of the American Meteorological Society* 78.11 (1997), pp. 2539–2558. DOI: [10.1175/1520-0477\(1997\)078<2539:GPAYMA>2.0.CO;2](https://doi.org/10.1175/1520-0477(1997)078<2539:GPAYMA>2.0.CO;2).
- [46] Richard E. Zeebe. "History of Seawater Carbonate Chemistry, Atmospheric CO₂, and Ocean Acidification". In: *Annual Review of Earth and Planetary Sciences* 40.1 (2012), pp. 141–165. DOI: [10.1146/annurev-earth-042711-105521](https://doi.org/10.1146/annurev-earth-042711-105521).
- [47] Richard E. Zeebe and Peter Westbroek. "A simple model for the CaCO₃ saturation state of the ocean: The "Strangelove," the "Neritan," and the "Cretan" Ocean". In: *Geochemistry, Geophysics, Geosystems* 4.12 (2003). DOI: [10.1029/2003GC000538](https://doi.org/10.1029/2003GC000538).
- [48] Richard E. Zeebe and Dieter Wolf-Gladrow. *CO₂ in Seawater: Equilibrium, kinetics, isotopes*. Jan. 2001. ISBN: 0 444 50946 1.